BNL-224588-2023-TECH
EIC-ADD-TN-065

Electron cloud thresholds at the arcs of the Electron-Ion Collider hadron storage ring

S. Verdu-Andres

June 2023

Electron-Ion Collider

Brookhaven National Laboratory

U.S. Department of Energy

USDOE Office of Science (SC), Nuclear Physics (NP) (SC-26)

DISCLAIMER

Electron cloud thresholds at the arcs of the Electron-Ion Collider hadron storage ring

Silvia Verdú-Andrés*
Brookhaven National Laboratory
Upton, NY 11973 (USA)
(EIC Project)
(Dated: September 15, 2023)

The Electron-Ion Collider is designed to provide high-luminosity collisions. For the highest luminosity scenario, the hadron storage ring will host a 275 GeV beam consisting of 1160 bunches with 6.9e10 protons per bunch. Previous work has found that some sections of the hadron storage ring will experience electron cloud buildup if their vacuum chamber does not show a sufficiently low secondary electron emission value. This technical note reviews the electron cloud growth thresholds for the updated screen profile and lattice.

I. INTRODUCTION

The Electron-Ion Collider (EIC) is designed to provide high-luminosity collisions. For the highest luminosity scenario, the hadron storage ring (HSR) will host a 275 GeV beam consisting of 1160 bunches with 6.9e10 protons per bunch, which entails a significantly short bunch spacing of only 10.15 ns. In the past, other proton accelerators with similar beam parameters have encountered electron cloud (the AGS [1] and RHIC [2–4] at BNL, the PS [5, 6], SPS [7] and LHC [8, 9] at CERN). Table I lists relevant beam parameters for some of these machines.

TABLE I. Beam parameters for proton accelerators where electron cloud was observed.

	RHIC	LHC	EIC HSR
Bunch spacing (ns)	108	50 – 25	10.15
Bunch charge (1e10 ppb)	13.5	11.5	6.9

Electron cloud can lead to adverse, undesired effects to the beam quality and stability if not addressed: sudden, large vacuum pressure rise, beam instabilities, emittance growth and blow-up, particle loss, interference with diagnostics, excessive heat on chamber walls, etc.. Previous work studied the electron cloud growth thresholds for the hadron storage ring of the EIC [10]. This technical note reviews the electron cloud growth thresholds for the updated screen profile and lattice.

A. Screen profile

The latest screen profile has a racetrack cross section. In the past, electron cloud thresholds were investigated for round and polygonal profiles [10]. These designs were abandoned with the adoption of the actively-cooled screen as a baseline. Fig. 1 shows the polygonal and racetrack profiles and Table II compares the heat load deposited by an electron cloud generated as result of the highest luminosity beam passage through an arc dipole's screen with a SEY = 1.3 surface for screens with different profile.

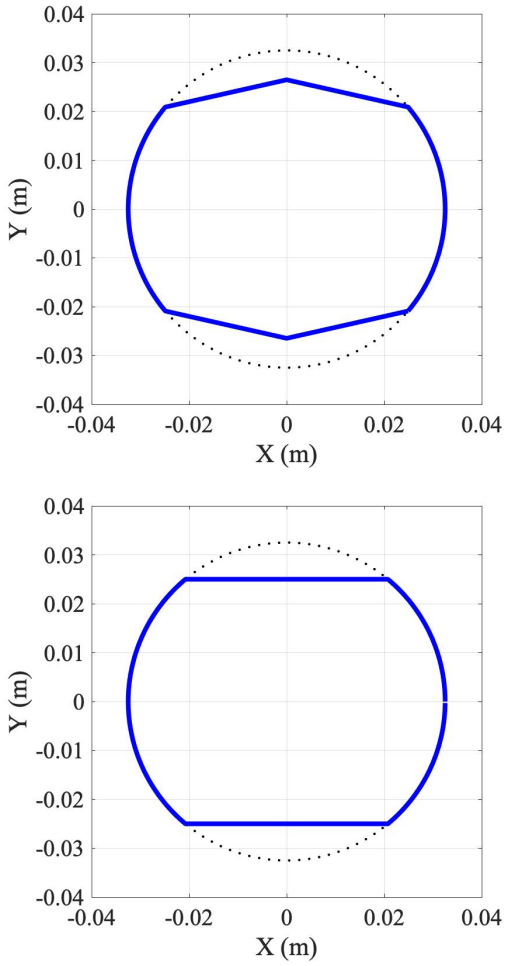

FIG. 1. Polygonal (top) and racetrack (bottom) profiles.

* sverdu@bnl.gov

B. Beam scenarios

Table III lists the proton beam scenarios studied in this technical note and their main parameter values. Ramp up from injection energy to store will be performed with the beam circulating on-center of the beam pipe. At store, the beam orbit aligns with the center of the EIC HSR vacuum chamber. For collisions, an offset of up to ±21 mm in a 69 mm diameter beam pipe for 275 GeV and 100 GeV beams is required for synchronicity of the electron bunches with ultra-relativistic proton bunches at the interaction point.

C. Magnet strengths and Twiss parameters

Magnet strengths and Twiss parameters of the most recent lattice EIC-HSR-220921a for the 275 GeV proton beams in store (on-axis) are listed in Table IV. The lattice for beams in collision is under preparation. In collision mode, the 275 GeV proton beams could circulate through the arcs with a maximum radial shift of 21 mm (F-HSR-SYS.5). The maximum orbit excursion will be at quadrupoles and sextupoles.

D. SEY curve model and parameter values

The electron cloud growth thresholds are determined by PyECLOUD [11] simulations. The simulations inspect how the electron cloud growth threshold varies in function of the SEY value (variable "SEY") using the default SEY curve model in the PyECLOUD code ('ECLOUD') [11, 12], with the model parameters taking the values shown in Table V for amorphous carbon [13]. The heat load deposited by the electron cloud is used as a monitor to determine the electron cloud growth threshold.

TABLE II. Heat load deposited from electron cloud generated by the passage of highest luminosity beam through arc dipole's screen with SEY = 1.3 surface for different screen cross sections.

Profile	Radius (mm)	Vertical aperture (mm)	Heat load (W/m)
Round	25.0	–	4.10
	32.5	–	8.03
	35.0	–	8.45
Polygonal	32.5	30.0	8.02
Racetrack	32.5	25.0	7.97

TABLE III. Proton beam parameter values for the highest center-of-mass energy (E_{CM}) and the highest luminosity ($\mathscr{L}$) beam scenarios.

Parameter	Highest E_{CM}	Highest $\mathscr{L}$
Species	p^+	p^+
Energy (GeV)	275	275
No. bunches	290	1160
Bunch spacing (ns)	40.59	10.15
Bunch charge (10^{10})	19.1	6.9
RMS bunch length (cm)	6	6
Center-of-Mass Energy (GeV)	140.7	104.9
Luminosity (10^{33} cm^{-2}s^{-1})	1.54	10

TABLE V. Parameters from PyECLOUD SEY curve model 'ECLOUD' and measured values for amorphous carbon [13].

R_0	0.7-0.9
E_0 (eV)	150
E_{max} (eV)	275.1
s	1.773
δ_{max} (variable "SEY")	1.06

II. ELECTRON CLOUD GROWTH THRESHOLDS FOR THE HSR ARCS WITH UPDATED SCREEN PROFILE AND LATTICE

A. Arc dipoles, quadrupoles and sextupole magnets

Figure 2 shows the heat load deposited by the electron cloud for the highest luminosity and highest Ecm beams when traveling 18 mm off-center. The highest luminosity beam – with 1160 bunches – shows lower SEY thresholds (around 1.02) than the highest Ecm beam – which contains 290 bunches with larger bunch charge. The screens at the arc quadrupoles show the lowest SEY threshold for the highest Ecm beam while those at the arc sextupoles show the lowest SEY threshold for the highest luminosity beam. The difference in SEY threshold for the focusing and defocusing magnets arises from differences in the magnet strength – see Table IV. The lowest SEY threshold for the arc dipoles is found when the highest luminosity beam travels on axis, as shown in Fig. 3.

Figures 4, 5 and 6 show the beam offset scans for the highest luminosity beam and the strongest gradient magnets of each type – the most demanding scenario. The electron cloud buildup response to different beam offsets depends on the magnet type. The known behaviour of higher order magnets as magnetic bottles is enhanced by the beam offset.

A low SEY is required for the vacuum chamber of the HSR superconducting magnets. The baseline plan is to apply a thin layer of amorphous carbon (SEY∼1, no need for activation by baking) to the screen. In prac-

TABLE IV. Magnet strengths and Twiss parameters of lattice EIC-HSR-220921a for 275 GeV proton beams in store (on-axis).

Parameter	Arc D	Arc QF	Arc SF	Arc D	Arc QD	Arc SD
Strength (T/m^n)	-3.782	-72.522	-368.877	-3.782	+74.275	+577.077
Order n	0	1	2	0	1	2
Length (m)	9.44	1.11	0.75	9.44	1.11	0.75
β_x (m)	39.72	11.48	11.63	14.38	48.20	47.65
β_y (m)	13.66	47.24	46.69	38.74	10.90	11.04
D_x (m)	1.1084	1.8951	1.8841	1.7172	1.0126	1.0185

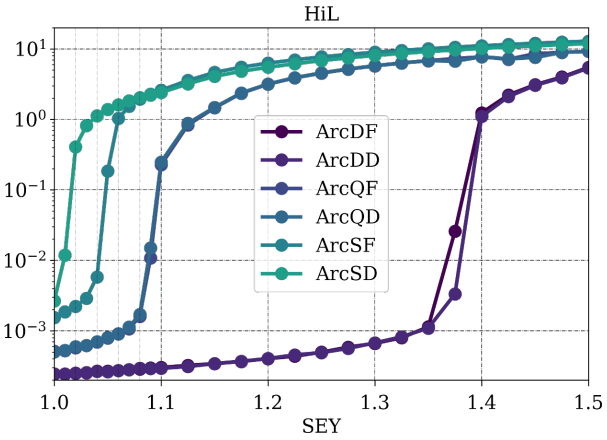

FIG. 2. Heat load due to electron cloud buildup for highest luminosity (top) and highest Ecm (bottom) beams traveling at 18 mm off-center.

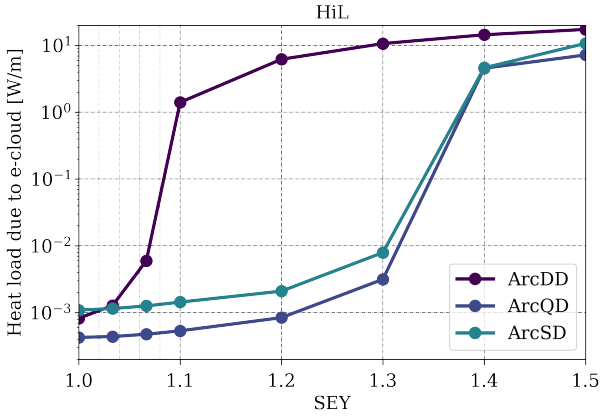

FIG. 3. Heat load due to electron cloud buildup for highest luminosity beam traveling on axis.

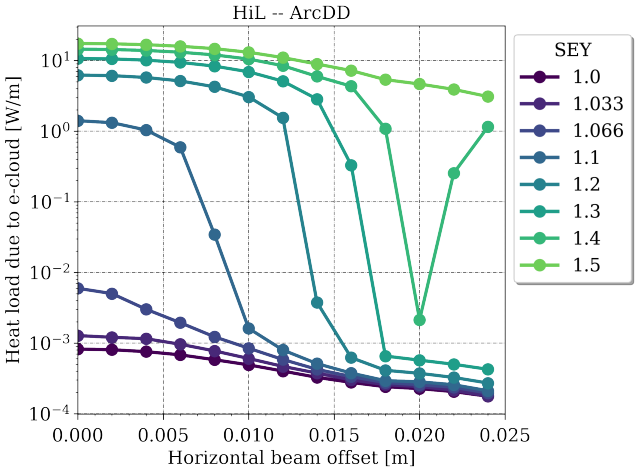

FIG. 4. Heat load due to electron cloud buildup for high luminosity beam in screens of the arc dipole magnets.

tice, the produced amorphous carbon films will feature an SEY that follows a bell curve like distribution [14, 15]. Physisorbed molecules on the amorphous carbon surface may also increase the apparent SEY [16]. Table VI lists the heat deposited by the electron cloud for selected SEY values. Scrubbing might be needed during commissioning / pre-operations and there should be some budget allocated to the heat deposited by the scrubbing beam. As the spatial distribution of delivered dose depends as well on the magnet type and beam offset, operation at different beam offsets entails consequences for the scrubbing campaign. Several scrubbing beams may be required to clear electron cloud in the superconducting arcs.

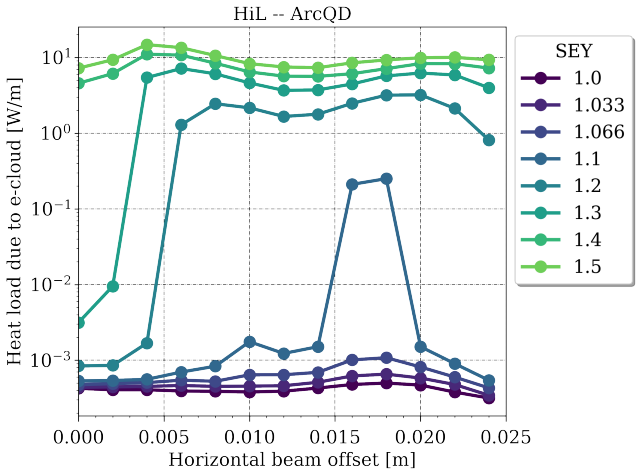

FIG. 5. Heat load due to electron cloud buildup for high luminosity beam in screens of the arc quadrupole defocusing magnets.

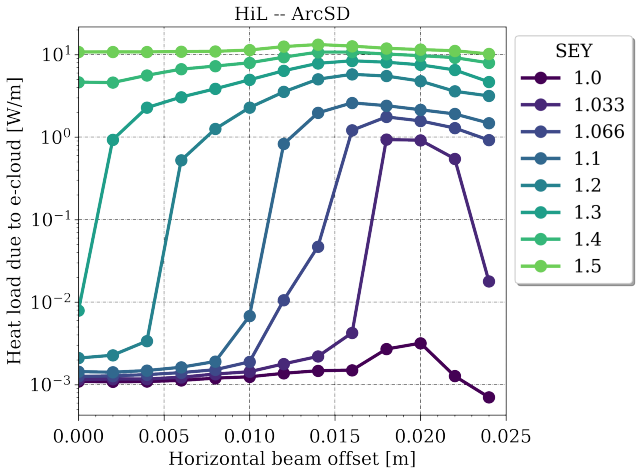

FIG. 6. Heat load due to electron cloud buildup for high luminosity beam in screens of the arc sextupole defocusing magnets.

B. Cold mass interconnects

The cold mass interconnects will host the new button beam position monitors (BPM) and the RF shielded bellows. In presence of no external fields and during operation with colliding (off-centered) beams, Fig. 7 shows that electron cloud will build up in presence of the highest luminosity beam for SEY values featured by conventional metallic surfaces like copper (up to 1.7) and scrubbed stainless steel (1.48).

The beam offset at the cold mass interconnects will vary in a broad range, depending on their position along the lattice. The lowest SEY threshold is found for the passage of the beam on-axis, as shown in Fig. 8.

TABLE VI. Heat loads (W/m) for selected SEY values of the screens at the magnets (from Fig. 2, 18 mm beam offset) and drifts (from Fig. 7, on-axis beam) of the HSR arcs.

SEY	1.1	1.2	1.3
Highest $\mathscr{L}$			
Drift	0.0040	3.4362	9.2767
Arc dipole	0.0003	0.0004	0.0007
Arc quadrupole	0.2478	3.1756	5.7655
Arc sextupole	2.4035	5.4965	8.0734
Highest E_{CM}			
Drift	0.0032	0.0037	0.0043
Arc dipole	0.0012	0.0015	0.0022
Arc quadrupole	0.0008	0.0017	0.5161
Arc sextupole	0.0017	0.0023	0.0047

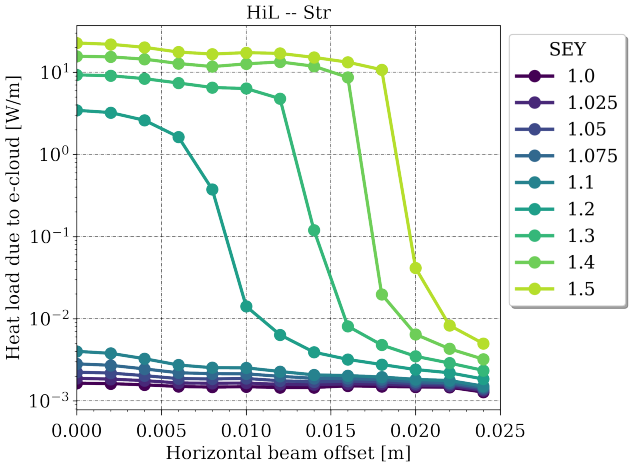

FIG. 7. Heat load due to electron cloud buildup by the highest luminosity beam for no field section with nominal aperture racetrack profile.

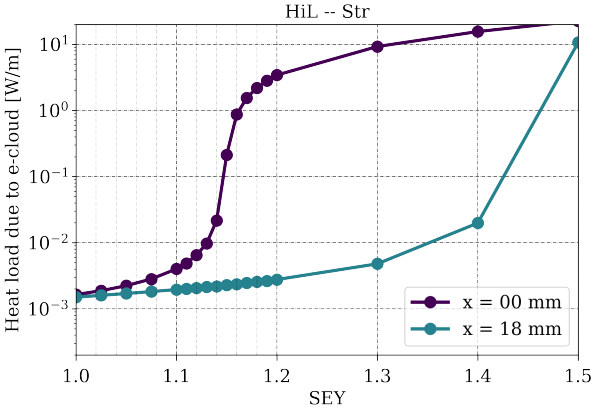

FIG. 8. Heat load due to electron cloud buildup by centered (x=0) and off-axis (x = 18 mm) highest luminosity beam (top) for no field section with nominal aperture racetrack profile.

The fringe fields of the magnets could make the electron cloud stronger. This result suggests that the surfaces exposed to the beam in the cold mass interconnects must have amorphous carbon coating or any other solution that shows a sufficiently low SEY to prevent electron cloud buildup. The HSR will be warmed up every year, with the fingers of the RF shielded bellows scratching against the edge of the cuff during thermal cycles and risk to flake if coated with amorphous carbon. The coating hardness should be assessed. From Fig. 9, the highest Ecm beam does not seem to build up an electron cloud.

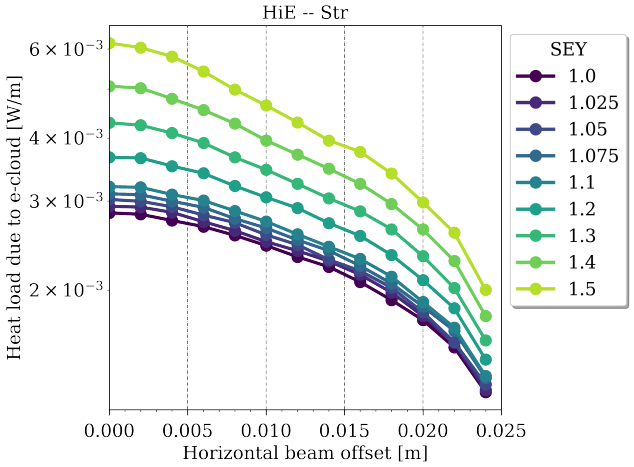

FIG. 9. Heat load due to electron cloud buildup by the highest Ecm beam for no field section with nominal aperture racetrack profile.

Figures 10 and 11 show the heat deposited by the electron cloud generated by the highest luminosity beam to the screen profile and to the 20-mm diameter BPM button which is farthest away from the beam for different SEY values of the racetrack profile chamber, respectively.

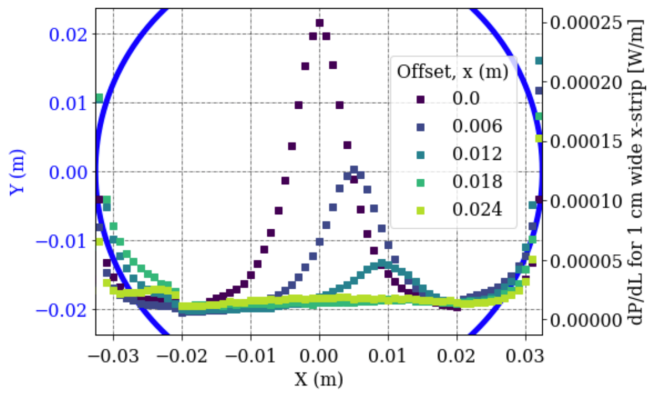

FIG. 10. Heat map along horizontal coordinate X of a nominal aperture racetrack profile with SEY = 1.1 due to electron cloud buildup by highest luminosity beam traveling at selected beam offsets x through no field region. The chamber profile is shown in blue.

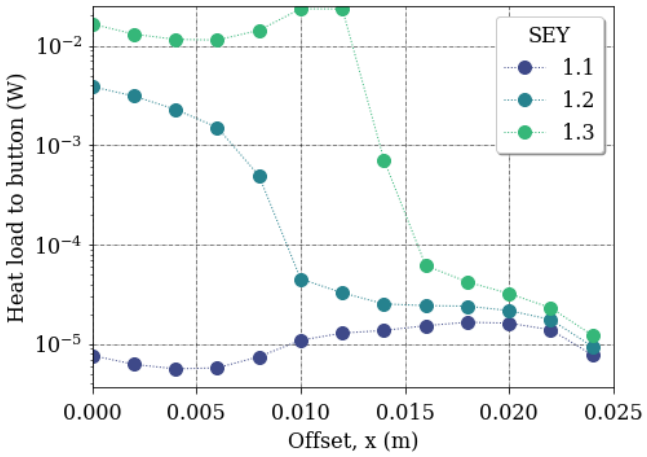

FIG. 11. Heat (W) deposited to a single 20 mm-diameter BPM button located at x = 26.2 mm by electron cloud from highest luminosity beam traveling through no-field region in a racetrack profile chamber. Worst case is for button farther away from the beam.

III. ELECTRON CLOUD GROWTH THRESHOLDS FOR D0 MAGNETS IN IR08

The present HSR design will use warm D0 magnets in all the straight sections. At the time of this study, a lattice solution for the D0s in IR08 was not available, so we assumed a value of 100 m for both beta functions and dispersion not larger than 10 cm, with a nominal field in the D0 of 3.698 T for the 275 GeV proton beam [17]. The D0 beam pipe is 89 mm diameter. Fig. 12 and 13 show the heat load deposited by electron cloud in the D0 magnets of IR08 computed for a 89 mm-diameter round chamber values in case a screen is deemed unnecessary. The results indicate that some low SEY (< 1.2) surface is needed to suppress electron cloud buildup in this region.

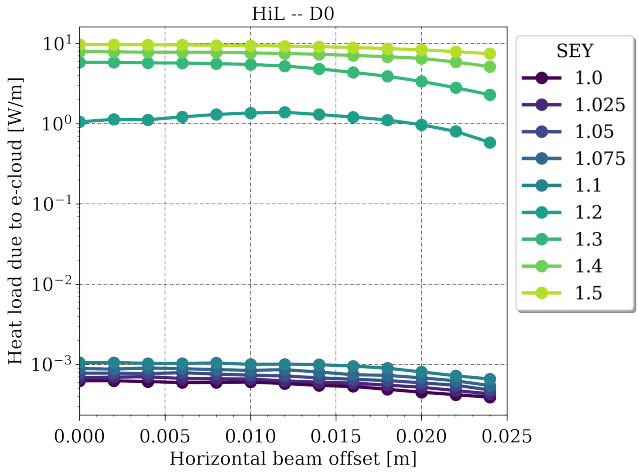

FIG. 12. Heat load due to electron cloud buildup for D0 magnets in IR08 (89 mm-diameter round profile).

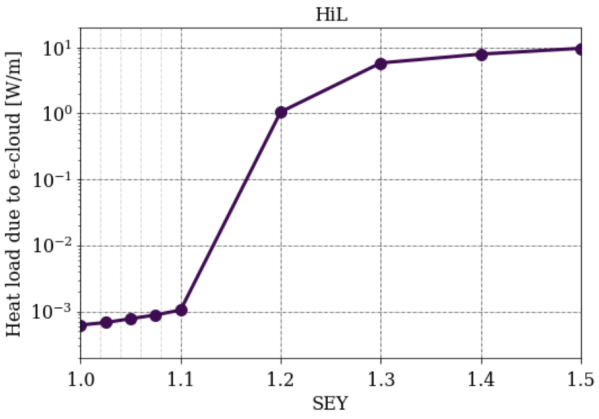

FIG. 13. Heat load due to electron cloud buildup for D0 magnets in IR08 (89 mm-diameter round profile) for centered highest luminosity beam in function of SEY.

IV. OVERVIEW

The results of this work are consistent with those presented in Ref. [10] for previous screen cross section and lattice parameters. While this work used the heat load deposited by the electron cloud to determine the electron cloud growth thresholds, next we will investigate the impact of the electron cloud on beam quality and stability, as well as mitigation strategies like the use of hybrid filling scheme beams. We also intend to investigate which are suited beam parameters for scrubbing campaigns.

ACKNOWLEDGMENTS

The author would like to thank Dean Hidas (BNL NSLS-II) for technical support to run the simulations, Scott Berg for providing lattice parameters and magnet strengths, Frederic Micolon and Pete Braunius for information about the BPM design, and Mike Blaskiewicz, Xiaofeng Gu, Guillaume Robert-Demolaize, and Vadim Ptitsyn for valuable discussions about electron cloud and the beam offset.

[1] E. C. Raka, The Nature Of The Transverse Instability In The Brookhaven AGS, in *6th International Conference on High-Energy Accelerators* (1967) pp. 428–430, https://inspirehep.net/files/60621ba177c461e4e9db5f473625b987.

[2] M. Blaskiewicz et al., The fast loss electron proton instability", proc. workshop on instabilities of high intensity hadron beams in rings, https://doi.org/10.1063/1.1303089.

[3] W. Fischer, J. M. Brennan, M. Blaskiewicz, and T. Satogata, Electron cloud measurements and simulations for the brookhaven relativistic heavy ion collider, Phys. Rev. ST Accel. Beams **5**, 124401 (2002).

[4] W. Fisher et al., Electron cloud experiments and cures in rhic, https://accelconf.web.cern.ch/p07/TALKS/TUXAB02_TALK.PDF.

[5] R. Cappi, M. Giovannozzi, E. Métral, G. Métral, G. Rumolo, and F. Zimmermann, Electron cloud buildup and related instability in the CERN Proton Synchrotron, Phys. Rev. ST Accel. Beams **5**, 094401 (2002).

[6] G. Rumolo, H. Bartosik, E. Belli, G. Iadarola, K. Li, L. Mether, A. Romano, and M. Schenk, Electron cloud in the CERN accelerator complex, in *57th ICFA Advanced Beam Dynamics Workshop on High-Intensity and High-Brightness Hadron Beams* (2016) p. TUAM4X01.

[7] G. Arduini, K. Cornelis, O. Grobner, N. Hilleret, W. Hofle, J. M. Jimenez, J. M. Laurent, G. Moulard, M. Pivi, and K. Weiss, Electron cloud: Observations with LHC-type beams in the SPS, in *7th European Particle Accelerator Conference (EPAC 2000)* (2000) pp. 939–941, https://accelconf.web.cern.ch/e00/papers/THP1B16.pdf.

[8] J. Wenninger, LHC commissioning and first operation at 6.5 TeV, Congrès Général SFP 2015 - Strasbourg: https://indico.ijclab.in2p3.fr/event/2956/contributions/6669/attachments/6224/7368/LHC.SFP.Aout15_JorgWenninger_v2_talk1.pdf.

[9] K. Li, H. Bartosik, G. Iadarola, L. Mether, A. Romano, G. Rumolo, and M. Schenk, Electron Cloud Observations during LHC Operation with 25 ns Beams, , TUPMW017 (2016).

[10] X. Gu, M. Blaskiewicz, A. Blednykh, G. Roberto-Demolaize, and S. Verdu-Andres, Electron Cloud Simulations for the Electron-Ion Collider in Brookhaven National Laboratory, EIC-ADD-TN-053; BNL-224221-2023-TECH (BNL, 2022) https://doi.org/10.2172/1969916.

[11] G. Iadarola, E. Belli, P. Dijkstal, L. Mether, A. Romano, G. Rumolo and E. Wulff, PyECLOUD Reference Manual (CERN, 2021) https://raw.githubusercontent.com/PyCOMPLETE/PyECLOUD/master/doc/reference/reference.pdf.

[12] G. Iadarola, *Electron cloud studies for CERN particle accelerators and simulation code development*, PhD dissertation, Università degli Studi di Napoli Federico II, Dipartimento di Ingegneria Elettrica e Tecnologie dell'Informazione (DIETI), Napoli, Italy (2014), https://cds.cern.ch/record/1705520/files/CERN-THESIS-2014-047_2.pdf.

[13] G. B. R. Salemme, V. Baglin and P. Chiggiato, Vacuum performance of amorphous carbon coating at cryogenic temperature with presence of proton beams (2016), proc. of IPAC'16, Busan, Korea, May 8-13, 2016 (JaCoW): 10.18429/JACoW-IPAC2016-THPMY007.

[14] M. Van Gompel et al., Amorphous carbon thin film coating of the sps beamline: Evaluation of the first coating implementation, https://inspirehep.net/literature/1626186.

[15] W. Vollenberg et al., Amourphous carbon coating in sps, https://cds.cern.ch/record/2809481/files/document.pdf.

[16] C. Yin-Vallgren, *Low Secondary Electron Yield Carbon Coatings for Electron Cloud Mitigation in Modern Particle Accelerators*, PhD Dissertation, CERN-THESIS-2011-063, Department of Fundamental Physics Chalmers University of Technology Göteborg, Sweden 2011 (2011), https://cds.cern.ch/record/1374938?ln=en.

[17] S. Berg, private communication on Nov. 23, 2022.